Wideband Dynamic Array-of-Subarrays Architecture for Extremely Large-Scale Antenna Array Systems

Seungnyun Kim* and Moe Z. Win†

*Wireless Information and Network Sciences Laboratory, Massachusetts Institute of Technology, Cambridge, MA, USA
†Laboratory for Information and Decision Systems, Massachusetts Institute of Technology, Cambridge, MA, USA

***Abstract*—Recently, wideband beamforming using extremely large-scale antenna array (ELAA) systems have gained much interest as a means to boost throughput in next generation (xG) networks. However, conventional phase shifter (PS)-based beamforming methods face challenges in wideband ELAA systems due to the beam squint effect, where beams at different frequencies become misaligned. Although the use of true time delay (TTD) can address this by creating frequency-dependent beamforming vectors, traditional TTD-based methods still experience considerable sidelobe leakage due to the mismatch between intended and generated beams. In this paper, we introduce a novel wideband beamforming architecture that dynamically configures connections between TTDs and PS subarrays using a switching network. By jointly optimizing subarray connections, TTD time delays, and PS phase shifts, wideband dynamic array-of-subarrays (WDAoSA) minimizes sidelobe gain and maximizes array gain in wideband ELAA systems. Numerical results show significant improvements in both array gain and data rate compared to conventional TTD-based methods.**

***Index Terms*—Wideband communications, beamforming, ELAA, near-field, array-of-subarrays (AoSA).**

I. Introduction

WIDEBAND communications exploiting millimeter-wave (mmWave) and terahertz (THz) band are key technologies of next generation (xG) networks to support data-intensive applications [1]. Despite their benefit, the major bottleneck of wideband communications is the significant signal attenuation due to path loss and molecular absorption. To compensate for the path loss, a beamforming operation realized by multi-antenna systems is essential [2]–[5]. Traditionally, phase shifters (PSs) that apply phase shifts independent of subcarrier frequency have been widely used for the beam generation. While these frequency-invariant beamforming techniques have been effective to some extent, they might not perform well in wideband systems due to the *beam squint effect*. The beam squint effect refers to a phenomenon where the array steering vectors vary across subcarriers, caused by the difference between the carrier and subcarrier frequencies [6]. Since the optimal beams aligned with the array steering vectors vary for each subcarrier, the frequency-invariant beamforming techniques suffer from severe data rate degradation in wideband systems.

The fundamental research described in this paper was supported, in part, by the National Research Foundation of Korea under Grant RS-2023-00252789, by the National Science Foundation under Grant CNS-2148251, by the federal agency and industry partners in the RINGS program, and by the Robert R. Taylor Professorship. (*Corresponding author: Moe Z. Win.*)

To address this issue, approaches that generate separate beams for each subcarrier using true time delays (TTDs), a unit comprising multiple switched delay lines, have gained much attention recently [7]–[12]. By selecting a delay line for radio-frequency (RF) signal propagation, TTD generates a phase shift proportional to the signal frequency. In [7], [8], partially-connected hybrid networks with one TTD connected to multiple PSs have been proposed. In [9], TTD-based hybrid precoding techniques have been proposed. In [10], [11], wideband beamforming techniques for near-field systems have been proposed. Also, in [12], a dynamic subarray architecture with fixed time delays has been proposed. A key challenge with conventional TTD-based beamforming techniques is that the partially-connected structure between TTDs and PSs results in an inevitable mismatch between the desired ultra-sharp pencil beams and the generated beams. This, together with the fixed connections betweenTTDs and PS subarrays, leads a significant degradation in array gain. One exception is the dynamic subarray structure proposed in [12], but in that approach, the time delays of the TTDs remain fixed and are not adequately adjusted to match varying wireless environments.

An aim of this paper is to propose a novel TTD-based beamforming architecture maximizing the array gain of wideband extremely large-scale antenna array (ELAA) systems. The key idea of the proposed scheme, referred to as *wideband dynamic array-of-subarrays* (WDAoSA), is to dynamically adjust the connections between TTDs and PS subarrays via a switch network, while jointly optimizing the TTD time delay and the PS phase shifts. By carefully selecting the TTDs connected to each PS subarray based on the wireless propagation environment, the proposed scheme can reduce the gap between the desired ultra-sharp pencil beamforming vectors and the generated frequency-dependent beamforming vectors. From the extensive simulations, we demonstrate that WDAoSA significantly improves the array gain over the conventional TTD-based beamforming schemes.

Notation: Random variables are displayed in sans serif, upright fonts; their realizations in serif, italic fonts. Vectors and matrices are denoted by bold lowercase and uppercase letters, respectively. For example, a random variable and its realization are denoted by x and x for scalars, $\mathbf{x}$ and $\boldsymbol{x}$ for vectors, and $\mathbf{X}$ and $\boldsymbol{X}$ for matrices. Sets and random sets are denoted by upright sans serif and calligraphic font, respectively. For example, a random set and its realization are denoted by X and $\mathcal{X}$, respectively. The m-by-n matrix of zeros is denoted

by $\mathbf{0}_{m\times n}$; when $n=1$, the m-dimensional vector of zeros is simply denoted by $\mathbf{0}_m$. The m-by-m identity matrix is denoted by $\boldsymbol{I}_m$. The operator $\|\boldsymbol{x}\|_2$ denotes the Euclidean norm. The operations $\otimes$ and $\odot$ denote the Kronecker product and the element-wise product, respectively. The transpose, conjugate, and conjugate transpose of $\boldsymbol{X}$ are denoted by $(\cdot)^{\mathrm{T}}$, $(\cdot)^*$, and $(\cdot)^{\mathrm{H}}$, respectively. The notations $\mathrm{diag}(\boldsymbol{x})$ and $\boldsymbol{x}^{(p)}$ represent a diagonal matrix with the arguments being its diagonal elements and a vector with the pth power of arguments being its elements, respectively.

II. Wideband ELAA Systems

A. Downlink Wideband ELAA System Model

We consider a downlink wideband ELAA system where a base station (BS) equipped with N uniform linear array (ULA) antennas serves a single-antenna user equipment (UE). We also consider an orthogonal frequency-division multiplexing (OFDM) system with the carrier frequency f_{c}, number of subcarriers S, and system bandwidth B. The BS is equipped with the analog beamforming architecture consisting of a single RF chain, T TTDs, and N PSs. The received signal $\mathsf{y}_s\in\mathbb{C}$ of UE at the sth subcarrier is given by

$$\mathsf{y}_s = \sqrt{P_{\mathrm{tx}}}\mathbf{h}_s^{\mathrm{H}}\boldsymbol{w}_s\mathsf{s}_s + \mathsf{n}_s \tag{1}$$

where P_{tx} is the BS transmission power, $\mathbf{h}_s\in\mathbb{C}^N$ is the downlink channel vector, $\boldsymbol{w}_s\in\mathbb{C}^N$ is the beamforming vector, s_s is the data symbol, and $\mathsf{n}_s\sim\mathcal{CN}(0,\sigma^2)$ is the Gaussian noise at the sth subcarrier. Then the data rate R of UE is

$$\mathsf{R} = \frac{1}{S}\sum_{s=1}^{S}\log_2\Big(1+\frac{P_{\mathrm{tx}}}{\sigma^2}\big|\mathbf{h}_s^{\mathrm{H}}\boldsymbol{w}_s\big|^2\Big). \tag{2}$$

We use the frequency-selective near-field channel model where the sth subcarrier channel vector $\mathbf{h}_s\in\mathbb{C}^N$ is expressed as

$$\mathbf{h}_s = \sqrt{\beta_s}\boldsymbol{a}_N(\boldsymbol{p}^{\mathrm{ue}},f_s) + \sqrt{\beta_s}\sum_{i=1}^{N_{\mathrm{p}}-1}\alpha_{s,i}\boldsymbol{a}_N(\boldsymbol{p}_i,f_s) \tag{3}$$

where N_{p} is the number of propagation paths, $f_s = f_{\mathrm{c}} - \frac{B}{2} + \frac{B(s-1)}{S-1}$ is the sth subcarrier frequency, and $\boldsymbol{p}^{\mathrm{ue}}$ is the position vector of UE. Also, $\beta_s = (\frac{c}{4\pi f_s r})^2 e^{-k(f_s)r}$ is the path loss accounting for the free space path loss and the molecular absorption with $k(f_s)$ being the absorption coefficient and $\alpha_{s,i}\sim\mathcal{CN}(0,\Gamma_i(f_s))$ is the path gain with $\Gamma_{k,i}(f_s)$ being the reflection coefficient [11], [13]. In addition, $\boldsymbol{p}_i$ is the position vector of the ith scatterer and $\boldsymbol{a}_N(\boldsymbol{p},f_s)$ is the $N\times 1$ near-field array steering vector at the sth subcarrier defined as $\boldsymbol{a}_N(\boldsymbol{p},f_s) = \big[e^{-j2\pi f_s\frac{\|\boldsymbol{p}-\boldsymbol{q}_1\|_2}{c}}e^{-j2\pi f_s\frac{\|\boldsymbol{p}-\boldsymbol{q}_2\|_2}{c}}\cdots e^{-j2\pi f_s\frac{\|\boldsymbol{p}-\boldsymbol{q}_N\|_2}{c}}\big]^{\mathrm{T}}$ where $\boldsymbol{q}_n\in\mathbb{R}^2$ is the position vector of the nth BS antenna and c is the speed of light. Then the array gain $G(\boldsymbol{w}_s,\boldsymbol{p})$ of the sth subcarrier beamforming vector $\boldsymbol{w}_s$ at direction $\boldsymbol{p}$ is

$$G(\boldsymbol{w}_s,\boldsymbol{p}) \triangleq \frac{1}{N}\boldsymbol{a}_N^{\mathrm{H}}(\boldsymbol{p},f_s)\,\boldsymbol{w}_s\,. \tag{4}$$

Note that $\boldsymbol{a}_N(\mathbf{p},f_s)$ depends on f_s. However, in the PS-based beamforming techniques, the beamforming vectors generated by PSs remain the same across all subcarriers. Due to this beam squint effect, the conventional PS-base approaches suffer from severe array gain degradation in wideband systems.

B. Conventional TTD-Based Beamforming

To mitigate the beam squint effect, beamforming approaches exploiting a combination of TTDs and PSs have been proposed [7]–[12]. Specifically, when using $T(<N)$ TTDs and N PSs, the TTD beamforming vector $\boldsymbol{w}_s^{\mathrm{ttd}}(\boldsymbol{\tau})\in\mathbb{C}^T$ at the sth subcarrier and the PS beamforming vector $\boldsymbol{w}^{\mathrm{ps}}(\boldsymbol{\theta})\in\mathbb{C}^N$ for given time delays $\boldsymbol{\tau} = [\,\tau_1\,\tau_2\,\cdots\,\tau_T\,]^{\mathrm{T}}$ and phase shifts $\boldsymbol{\theta} = [\,\theta_1\,\theta_2\,\cdots\,\theta_N\,]^{\mathrm{T}}$ are defined as

$$\boldsymbol{w}_s^{\mathrm{ttd}}(\boldsymbol{\tau}) \triangleq \big[\,e^{-j2\pi f_s\tau_1}\;e^{-j2\pi f_s\tau_2}\;\cdots\;e^{-j2\pi f_s\tau_T}\,\big]^{\mathrm{T}}. \tag{5}$$

$$\boldsymbol{w}^{\mathrm{ps}}(\boldsymbol{\theta}) \triangleq \big[\,e^{-j\theta_1}\;e^{-j\theta_2}\;\cdots\;e^{-j\theta_N}\,\big]^{\mathrm{T}}. \tag{6}$$

In the conventional TTD-based beamforming schemes, the time delays of T TTDs and the phase shifts of N PSs are configured as $\boldsymbol{\tau}^{\mathrm{pc}} \triangleq \big[\,\frac{\|\boldsymbol{p}-\boldsymbol{q}_P\|_2}{c}\;\frac{\|\boldsymbol{p}-\boldsymbol{q}_{2P}\|_2}{c}\;\cdots\;\frac{\|\boldsymbol{p}-\boldsymbol{q}_{TP}\|_2}{c}\,\big]$ and $\boldsymbol{\theta}^{\mathrm{pc}} \triangleq 2\pi f_c\big[\,\frac{\|\boldsymbol{p}-\boldsymbol{q}_1\|_2}{c}\;\frac{\|\boldsymbol{p}-\boldsymbol{q}_2\|_2}{c}\;\cdots\;\frac{\|\boldsymbol{p}-\boldsymbol{q}_N\|_2}{c}\,\big] - \big(2\pi f_c\boldsymbol{\tau}^{\mathrm{pc}}\big)\otimes\mathbf{1}_P$ so that the corresponding beamforming vector $\boldsymbol{w}_s^{\mathrm{pc}}\in\mathbb{C}^N$ at the sth subcarrier resembles an array steering vector:

$$\begin{aligned}\boldsymbol{w}_s^{\mathrm{pc}} &\triangleq \boldsymbol{w}^{\mathrm{ps}}(\boldsymbol{\theta}^{\mathrm{pc}})\odot\big(\boldsymbol{w}_s^{\mathrm{ttd}}(\boldsymbol{\tau}^{\mathrm{pc}})\otimes\mathbf{1}_P\big)\\ &= \boldsymbol{a}_N(\boldsymbol{p},f_c)\odot\\ &\quad\left(\left[\frac{[\boldsymbol{a}_N(\boldsymbol{p},f_s)]_{tP}}{[\boldsymbol{a}_N(\boldsymbol{p},f_c)]_{tP}}\;\middle|\;t=1,2,\ldots,T\right]^{\mathrm{T}}\otimes\mathbf{1}_P\right).\end{aligned} \tag{7}$$

One can observe that when $f_s=f_c$, the relationship $\boldsymbol{w}_s^{\mathrm{pc}} = \boldsymbol{w}_s^{\mathrm{fc}}$ holds; however, this equality breaks down when $f_s\neq f_c$. This discrepancy results in reduced array gain $G(\boldsymbol{w}_s,\boldsymbol{p})$ and lower data rate R. In fact, the mismatch between $\boldsymbol{w}s^{\mathrm{pc}}$ and $\boldsymbol{w}_s^{\mathrm{fc}}$ becomes more significant as $|f_s-f_c|$ increases, causing substantial sidelobe leakage in the subcarrier beams.

III. Wideband Dynamic Array-of-Subarray Architecture

Recall that conventional partially-connected structure suffers from significant array gain degradation due to the fixed connections between TTDs and PS subarrays. To handle this issue, WDAoSA exploits a switch network between the TTD subarray and the PS subarrays. Using the switch network, WDAoSA dynamically configures the subarray connection as well as the TTD time delays and PS phase shifts to maximize the array gain. Furthermore, to reduce the computational complexity caused by the large number of antennas, we develop a distributed beamforming optimization framework that optimizes the subarray connection and the TTD time delays in a centralized manner while the PS phase shifts are optimized in a distributed manner at the subarray level.

A. WDAoSA Network Architecture

The proposed WDAoSA consists of three major components: 1) a TTD network with T TTDs; 2) a switch network; and 3) a PS network with N PSs (see Fig. 1). The N PSs are divided into L subarrays, each consisting of $\frac{N}{L}=K$ PSs and a single-pole multiple-throw (SPMT) switch that can be connected to one of TTDs. The subarray connection is expressed by the subarray connection matrix $\boldsymbol{E}_{\boldsymbol{\pi}} \triangleq [\,\boldsymbol{e}_{\pi_1}\,\boldsymbol{e}_{\pi_2}\,\cdots\,\boldsymbol{e}_{\pi_L}\,]$. Let $\boldsymbol{\pi} = [\,\pi_1\,\pi_2\,\cdots\,\pi_L\,]^{\mathrm{T}}$ be the subarray connection vector

where $\pi_l \in \mathcal{T}$ is the index of TTD connected to the lth PS subarray. Also, let $\boldsymbol{\tau} = [\,\tau_1\,\tau_2\,\cdots\,\tau_T\,]^{\mathrm{T}}$ and $\boldsymbol{\theta} = [\,\theta_1\,\theta_2\,\cdots\,\theta_N\,]^{\mathrm{T}}$ be the time delay and phase shift vectors where τ_t and θ_n are the time delay and the phase shift of the tth TTD and the nth PS, respectively. Then the WDAoSA beamforming vector $\boldsymbol{w}_s \in \mathbb{C}^N$ at the sth subcarrier is

$$\boldsymbol{w}_s \triangleq \boldsymbol{w}^{\mathrm{ps}}(\boldsymbol{\theta}) \odot \left(\left(\boldsymbol{E}_{\boldsymbol{\pi}}^{\mathrm{T}} \boldsymbol{w}_s^{\mathrm{ttd}}(\boldsymbol{\tau}) \right) \otimes \mathbf{1}_K \right). \tag{8}$$

We now explain the decomposition of array gain, which is crucial for the distributed beamforming optimization framework. Let $\mathcal{N}_t \triangleq \{(l-1)K+k \in \mathcal{N} \mid \pi_l = t, k = 1,2,\ldots,K\}$ be the set of antenna element indices connected to the tth TTD. Also, let $\boldsymbol{a}_{N,t}(\boldsymbol{p}, f_s) \in \mathbb{C}^{|\mathcal{N}_t|}$ and $\boldsymbol{w}_{s,t} \in \mathbb{C}^{|\mathcal{N}_t|}$ be the corresponding subvectors of $\boldsymbol{a}_N(\boldsymbol{p}, f_s)$ and $\boldsymbol{w}_s$, respectively:

$$\boldsymbol{a}_{N,t}(\boldsymbol{p}, f_s) \triangleq \left[[\boldsymbol{a}_N(\boldsymbol{p}, f_s)]_n \,\middle|\, n \in \mathcal{N}_t \right]^{\mathrm{T}} \tag{9}$$

$$\boldsymbol{w}_{s,t} \triangleq \left[[\boldsymbol{w}_s]_n \,\middle|\, n \in \mathcal{N}_t \right]^{\mathrm{T}} = e^{-j2\pi f_s \tau_t} \boldsymbol{w}^{\mathrm{ps}}(\boldsymbol{\theta}_{\mathcal{N}_t}) \tag{10}$$

where $\boldsymbol{\theta}_{\mathcal{N}_t} \triangleq [\theta_n \mid n \in \mathcal{N}_t]^{\mathrm{T}}$ is the corresponding subvector of $\boldsymbol{\theta}$. Then the tth subarray gain $G_t(\boldsymbol{w}_{s,t}, \boldsymbol{p})$ of $\boldsymbol{w}_{s,t}$ at the target direction $\boldsymbol{p}$ is defined as

$$\begin{aligned} G_t(\boldsymbol{w}_{s,t}, \boldsymbol{p}) &\triangleq \boldsymbol{a}_{N,t}^{\mathrm{H}}(\boldsymbol{p}, f_s)\, \boldsymbol{w}_{s,t} \\ &= e^{-j2\pi f_s \tau_t} \boldsymbol{a}_{N,t}^{\mathrm{H}}(\boldsymbol{p}, f_s)\, \boldsymbol{w}^{\mathrm{ps}}(\boldsymbol{\theta}_{\mathcal{N}_t}). \end{aligned} \tag{11}$$

Then $G(\boldsymbol{w}_s, \boldsymbol{p})$ is expressed as a sum of $\{G_t(\boldsymbol{w}_{s,t}, \boldsymbol{p})\}_{t=1}^T$ as $G(\boldsymbol{w}_s, \boldsymbol{p}) = \sum_{t=1}^T \boldsymbol{a}_{N,t}^{\mathrm{H}}(\boldsymbol{p}, f_s)\, \boldsymbol{w}_{s,t} = \sum_{t=1}^T G_t(\boldsymbol{w}_{s,t}, \boldsymbol{p})$.

Remark 1. *Let $m_{s,t}$ and $v_{s,t}$ be the magnitude and argument of the tth subarray gain $G_t(\boldsymbol{w}_{s,t}, \boldsymbol{p})$. Then $m_{s,t}$ is a sole function of $\boldsymbol{\theta}_{\mathcal{N}_t}$, whereas $v_{s,t}$ is determined by τ_t and $\boldsymbol{\theta}_{\mathcal{N}_t}$.*

$$\begin{aligned} m_{s,t} &\triangleq |G_t(\boldsymbol{w}_{s,t}, \boldsymbol{p})| \\ &= \left| \boldsymbol{a}_{N,t}^{\mathrm{H}}(\boldsymbol{p}, f_s)\, \boldsymbol{w}^{\mathrm{ps}}(\boldsymbol{\theta}_{\mathcal{N}_t}) \right| \end{aligned} \tag{12}$$

$$\begin{aligned} v_{s,t} &\triangleq \angle G_t(\boldsymbol{w}_{s,t}, \boldsymbol{p}) \\ &= -2\pi f_s \tau_t + \angle\left(\boldsymbol{a}_{N,t}^{\mathrm{H}}(\boldsymbol{p}, f_s)\, \boldsymbol{w}^{\mathrm{ps}}(\boldsymbol{\theta}_{\mathcal{N}_t}) \right). \end{aligned} \tag{13}$$

Remark 1 suggests that the array gain maximization can be split into separate subarray gain maximization problems by treating $m_{s,t}$ and $v_{s,t}$ as independent variables. Building on this, we formulate the beamforming optimization problem as

$$\mathscr{P}_0: \quad \underset{\boldsymbol{\pi}, \boldsymbol{\tau}, \{\boldsymbol{\theta}_{\mathcal{N}_t}\}_{t=1}^T}{\text{maximize}} \quad \sum_{s=1}^S |G(\boldsymbol{w}_s, \boldsymbol{p})|^2 \tag{14a}$$

$$\text{subject to} \quad \pi_l \in \mathcal{T} \qquad \forall l \in \mathcal{L}. \tag{14b}$$

To solve $\mathscr{P}_0$, we use an alternating approach that first fixes $\{\boldsymbol{\theta}_{\mathcal{N}_t}\}_{t=1}^T$ and optimizes $(\boldsymbol{\pi}, \boldsymbol{\tau})$ in a centralized manner. We then fix $(\boldsymbol{\pi}, \boldsymbol{\tau})$ and optimize $\{\boldsymbol{\theta}_{\mathcal{N}_t}\}_{t=1}^T$ in a distributed manner.

B. Subarray Connection Optimization

For a given $(\boldsymbol{\tau}, \{\boldsymbol{\theta}_{\mathcal{N}_t}\}_{t=1}^T) = (\boldsymbol{\tau}^{\mathrm{opt}}, \{\boldsymbol{\theta}_{\mathcal{N}_t}^{\mathrm{opt}}\}_{t=1}^T)$, $\mathscr{P}_0$ is reduced to the subarray connection problem $\mathscr{P}_{0,\mathrm{a}}$ as

$$\mathscr{P}_{0,\mathrm{a}}: \quad \underset{\boldsymbol{\pi}}{\text{maximize}} \quad \sum_{s=1}^S \left| \boldsymbol{a}_N^{\mathrm{H}}(\boldsymbol{p}, f_s)\, \boldsymbol{w}_s \right|^2 \tag{15a}$$

$$\text{subject to} \quad \pi_l \in \mathcal{T} \qquad \forall l \in \mathcal{L}. \tag{15b}$$

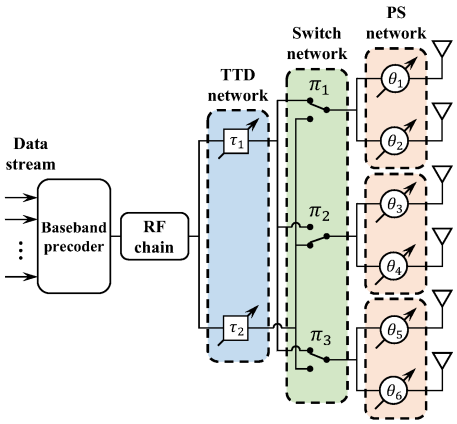

Fig. 1: Illustration of WDAoSA architecture.

Basically, $\mathscr{P}_{0,\mathrm{a}}$ is a combinatorial optimization problem that requires an exhaustive search to determine the optimal solution. To solve the problem at hand, we define a sparse subarray connection matrix $\tilde{\boldsymbol{E}} \triangleq [\,\tilde{\boldsymbol{e}}_1\,\tilde{\boldsymbol{e}}_2\,\cdots\,\tilde{\boldsymbol{e}}_L\,]$ where $\tilde{\boldsymbol{e}}_l$ is a sparse $T \times 1$ vector such that $[\tilde{\boldsymbol{e}}_l]_t = 1$ if $t = \pi_l$ and $[\tilde{\boldsymbol{e}}_l]_t = 0$ otherwise. Then π_l can be expressed as $\pi_l = \mathrm{supp}(\tilde{\boldsymbol{e}}_l)$. Using $\tilde{\boldsymbol{E}}$, we can re-express $\boldsymbol{w}_s$ as $\boldsymbol{w}_s = \boldsymbol{A}\tilde{\boldsymbol{E}}^{\mathrm{T}}\boldsymbol{b}_s$ where $\boldsymbol{A} \triangleq \mathrm{diag}(\boldsymbol{w}^{\mathrm{ps}}(\boldsymbol{\theta}^{\mathrm{opt}}))(\boldsymbol{I}_L \otimes \mathbf{1}_K)$ and $\boldsymbol{b}_s \triangleq \boldsymbol{w}_s^{\mathrm{ttd}}(\boldsymbol{\tau}^{\mathrm{opt}})$. Then we obtain the sparse recovery problem $\mathscr{P}_{1,\mathrm{a}}$ as

$$\mathscr{P}_{1,\mathrm{a}}: \quad \underset{\tilde{\boldsymbol{E}}}{\text{maximize}} \quad \sum_{s=1}^S \left| \boldsymbol{a}_N^{\mathrm{H}}(\boldsymbol{p}, f_s)\, \boldsymbol{A}\tilde{\boldsymbol{E}}^{\mathrm{T}}\boldsymbol{b}_s \right|^2 \tag{16a}$$

$$\text{subject to} \quad \|\tilde{\boldsymbol{e}}_l\|_0 \leqslant 1 \qquad \forall l \in \mathcal{L} \tag{16b}$$

$$\mathbf{1}_T^{\mathrm{T}}\tilde{\boldsymbol{e}}_l \leqslant 1 \qquad \forall l \in \mathcal{L} \tag{16c}$$

Unfortunately, $\mathscr{P}_{1,\mathrm{a}}$ is still nonconvex due to the ℓ_0-norm. To handle this issue, we use reweighted ℓ_2-norm approximation (RLA) that approximates $\|\tilde{\boldsymbol{e}}_l\|_0$ into ℓ_2-norm as [14]

$$\|\tilde{\boldsymbol{e}}_l\|_0 \approx \|\boldsymbol{P}_l\tilde{\boldsymbol{e}}_l\|_2^2 \tag{17}$$

where $\boldsymbol{P}_l \triangleq \mathrm{diag}(\sqrt{p_{1,l}}, \sqrt{p_{2,l}}, \cdots, \sqrt{p_{T,l}})$ and $p_{t,l} = \frac{1}{|[\tilde{\boldsymbol{e}}_l^{\mathrm{prev}}]_t|^2 + \epsilon^{-1}}$ is the RLA weight obtained from $\tilde{\boldsymbol{E}}^{\mathrm{prev}}$ of the previous RLA iteration. By allocating larger RLA weights to the smaller elements and progressively updating these weights, RLA penalizes these smaller elements, pushing them toward zero. By substituting (16b) with (17), we obtain

$$\mathscr{P}_{2,\mathrm{a}}: \quad \underset{\tilde{\boldsymbol{E}}}{\text{maximize}} \quad \sum_{s=1}^S \left| \boldsymbol{a}_N^{\mathrm{H}}(\boldsymbol{p}, f_s)\, \boldsymbol{A}\tilde{\boldsymbol{E}}^{\mathrm{T}}\boldsymbol{b}_s \right|^2 \tag{18a}$$

$$\text{subject to} \quad \|\boldsymbol{P}_l\tilde{\boldsymbol{e}}_l\|_2^2 \leqslant 1 \qquad \forall l \in \mathcal{L} \tag{18b}$$

$$\mathbf{1}_T^{\mathrm{T}}\tilde{\boldsymbol{e}}_l \leqslant 1 \qquad \forall l \in \mathcal{L}. \tag{18c}$$

Since $\mathscr{P}_{2,\mathrm{a}}$ is still nonconvex, we use successive convex approximation (SCA) to solve the problem [15]. We first re-express the objective function (18a) of $\mathscr{P}_{2,\mathrm{a}}$ as

$$f_{\mathrm{a}}(\tilde{\boldsymbol{E}}) \triangleq \sum_{s=1}^S \left| \boldsymbol{a}_N^{\mathrm{H}}(\boldsymbol{p}, f_s)\, \boldsymbol{A}\tilde{\boldsymbol{E}}^{\mathrm{T}}\boldsymbol{b}_s \right|^2 = \left\| \boldsymbol{D}^{\mathrm{T}} \mathrm{vec}(\tilde{\boldsymbol{E}}) \right\|_2^2 \tag{19}$$

where $\boldsymbol{D}_s \triangleq \left[\Re\{ (\boldsymbol{A}^{\mathrm{T}}\boldsymbol{a}_N^*(\boldsymbol{p}, f_s)) \otimes \boldsymbol{b}_s \}\, \Im\{ (\boldsymbol{A}^{\mathrm{T}}\boldsymbol{a}_N^*(\boldsymbol{p}, f_s)) \otimes \boldsymbol{b}_s \} \right]$ and $\boldsymbol{D} \triangleq [\,\boldsymbol{D}_1\,\boldsymbol{D}_2\,\cdots\,\boldsymbol{D}_S]$. Then, for a given $\tilde{\boldsymbol{E}}^{\mathrm{prev}}$ of previous SCA iteration, the linear approximation of f_{a} is

$$F\big(\tilde{\boldsymbol{E}} \mid \tilde{\boldsymbol{E}}^{\mathrm{prev}}\big) \triangleq f_{\mathrm{a}}\big(\tilde{\boldsymbol{E}}\big) + \nabla^{\mathrm{T}}_{\mathrm{vec}(\tilde{\boldsymbol{E}})} f\big(\tilde{\boldsymbol{E}}^{\mathrm{prev}}\big)\mathrm{vec}\big(\tilde{\boldsymbol{E}} - \tilde{\boldsymbol{E}}^{\mathrm{prev}}\big)$$
$$= 2\sum_{l=1}^{L} \boldsymbol{d}_l^{\mathrm{T}} \tilde{\boldsymbol{e}}_l - \big\|\boldsymbol{D}^{\mathrm{T}}\mathrm{vec}\big(\tilde{\boldsymbol{E}}^{\mathrm{prev}}\big)\big\|_2^2 \tag{20}$$

where $\boldsymbol{D}\boldsymbol{D}^{\mathrm{T}}\mathrm{vec}\big(\tilde{\boldsymbol{E}}^{\mathrm{prev}}\big) = [\,\boldsymbol{d}_1^{\mathrm{T}}\ \boldsymbol{d}_2^{\mathrm{T}}\ \cdots\ \boldsymbol{d}_L^{\mathrm{T}}\,]^{\mathrm{T}}$. By substituting $f(\tilde{\boldsymbol{E}})$ with $F(\tilde{\boldsymbol{E}} \mid \tilde{\boldsymbol{E}}^{\mathrm{prev}})$, we obtain

$$\mathscr{P}_{3,\mathrm{a}}: \quad \underset{\tilde{\boldsymbol{E}}}{\text{maximize}} \quad \sum_{l=1}^{L} \boldsymbol{d}_l^{\mathrm{T}} \tilde{\boldsymbol{e}}_l \tag{21a}$$
$$\text{subject to} \quad \|\tilde{\boldsymbol{e}}_l\|_0 \leqslant 1 \qquad \forall l \in \mathcal{L} \tag{21b}$$
$$\mathbf{1}_T^{\mathrm{T}} \tilde{\boldsymbol{e}}_l \leqslant 1 \qquad \forall l \in \mathcal{L}\,. \tag{21c}$$

Since $f_{\mathrm{a}}(\tilde{\boldsymbol{E}})$ is convex, $F(\tilde{\boldsymbol{E}} \mid \tilde{\boldsymbol{E}}^{\mathrm{prev}}) \leqslant f(\tilde{\boldsymbol{E}})$ and thus, the optimal value of $\mathscr{P}_{3,\mathrm{a}}$ is a lower bound of that of $\mathscr{P}_{2,\mathrm{a}}$. When ignoring (21b), the optimal solution $\{\tilde{\boldsymbol{e}}_l^{\mathrm{opt}}\}_{l=1}^{L}$ of $\mathscr{P}_{3,\mathrm{a}}$ is

$$\tilde{\boldsymbol{e}}_l^{\mathrm{opt}} = \begin{cases} \boldsymbol{e}_{t_{\max}} & \text{if } [\boldsymbol{d}_l]_{t_{\max}} > 0 \\ \boldsymbol{0}_T & \text{otherwise} \end{cases} \tag{22}$$

where $t_{\max} = \arg\max_{t\in\mathcal{T}} [\boldsymbol{d}_l]_t$. Since $\tilde{\boldsymbol{e}}_l^{\mathrm{opt}}$ has at most one nonzero element, it satisfies the sparsity constraint (21b), meaning that $\{\tilde{\boldsymbol{e}}_l^{\mathrm{opt}}\}_{l=1}^{L}$ is the optimal solution of $\mathscr{P}_{3,\mathrm{a}}$. The SCA iterations are repeated until $\tilde{\boldsymbol{E}}$ converges. Once $\tilde{\boldsymbol{E}}$ is obtained, we can get $\boldsymbol{\pi}^{\mathrm{opt}}$ as $\pi_t^{\mathrm{opt}} = \mathrm{supp}\big(\tilde{\boldsymbol{e}}_l\big)$.

C. TTD Time Delay Optimization

For a given $(\boldsymbol{\pi}, \{\boldsymbol{\theta}_{\mathcal{N}_t}\}_{t=1}^{T}) = (\boldsymbol{\pi}^{\mathrm{opt}}, \{\boldsymbol{\theta}_{\mathcal{N}_t}^{\mathrm{opt}}\}_{t=1}^{T})$, $\mathscr{P}_0$ is reduced to the time delay control problem $\mathscr{P}_{0,\mathrm{b}}$ as

$$\mathscr{P}_{0,\mathrm{b}}: \underset{\boldsymbol{\tau}}{\text{maximize}} \quad \sum_{s=1}^{S}\left|\sum_{t=1}^{T} m_{s,t} e^{j v_{s,t}}\right|^2 \tag{23a}$$
$$\text{subject to} \quad v_{s,t} = \angle(\boldsymbol{a}_{N,t}^{\mathrm{H}}(\boldsymbol{p}, f_s)\, \boldsymbol{w}^{\mathrm{ps}}(\boldsymbol{\theta}_{\mathcal{N}_t}^{\mathrm{opt}})) - 2\pi f_s \tau_t \quad \forall s \in \mathcal{S}, \forall t \in \mathcal{T} \tag{23b}$$

where $m_{s,t} = \big|\boldsymbol{a}_{N,t}^{\mathrm{H}}(\boldsymbol{p}, f_s)\, \boldsymbol{w}^{\mathrm{ps}}(\boldsymbol{\theta}_{\mathcal{N}_t}^{\mathrm{opt}})\big|$. Since the elements of the TTD beamforming vector generated from $\boldsymbol{\pi}$ have unit-modulus, one cannot uniquely determine $\boldsymbol{\tau}$ due to the phase ambiguity issue. To handle this issue, we redefine $\tilde{\boldsymbol{\tau}} = \big[\, e^{-jf_c\tau_1}\, e^{-jf_c\tau_2}\ \cdots\ e^{-jf_c\tau_T}\,\big]^{\mathrm{T}}$ to obtain $\mathscr{P}_{1,\mathrm{b}}$ as

$$\mathscr{P}_{1,\mathrm{b}}: \quad \underset{\tilde{\boldsymbol{\tau}}\in\mathcal{C}^T}{\text{maximize}} \quad \sum_{s=1}^{S}\left|\boldsymbol{m}_s^{\mathrm{T}} \boldsymbol{P}_s \tilde{\boldsymbol{\tau}}^{\left(2\pi\frac{f_s}{f_c}\right)}\right|^2 \tag{24a}$$
$$\text{subject to} \quad |[\tilde{\boldsymbol{\tau}}]_t| = 1 \qquad \forall t \in \mathcal{T}. \tag{24b}$$

Due to the unit-modulus constraints (24b), $\mathscr{P}_{3,\mathrm{b}}$ is nonconvex. To address these constraints, we leverage the fact that the set of unit-modulus vectors lies on a Riemannian manifold, which is a generalization of Euclidean space that allows the definition of differentiable structures on curved and abstract spaces. Specifically, by defining the set of T-dimensional unit-modulus vectors as $\mathcal{C}^T \triangleq \big\{\tilde{\boldsymbol{\tau}} \in \mathbb{C}^T \mid |[\tilde{\boldsymbol{\tau}}]_t| = 1, \forall t\big\}$, $\mathscr{P}_{0,\mathrm{b}}$ is recast to the unconstrained problem on $\mathcal{C}^T$ as

$$\mathscr{P}_{2,\mathrm{b}}: \quad \underset{\tilde{\boldsymbol{\tau}}\in\mathcal{C}^T}{\text{maximize}} \quad \sum_{s=1}^{S}\left|\boldsymbol{m}_s^{\mathrm{T}} \boldsymbol{P}_s \tilde{\boldsymbol{\tau}}^{\left(2\pi\frac{f_s}{f_c}\right)}\right|^2 \tag{25}$$

where $\boldsymbol{m}_s \in \mathbb{R}^T$ and $\boldsymbol{P}_s \in \mathbb{C}^{T\times T}$ are defined as

$$\boldsymbol{m}_s \triangleq [\, m_{s,1}\ m_{s,2}\ \cdots\ m_{s,T}\,]^{\mathrm{T}} \tag{26}$$
$$\boldsymbol{P}_s \triangleq \mathrm{diag}\big(e^{j\angle(\boldsymbol{a}_{N,1}^{\mathrm{H}}(\boldsymbol{p},f_s)\,\boldsymbol{w}^{\mathrm{ps}}(\boldsymbol{\theta}_{\mathcal{N}_1}))}, e^{j\angle(\boldsymbol{a}_{N,2}^{\mathrm{H}}(\boldsymbol{p},f_s)\,\boldsymbol{w}^{\mathrm{ps}}(\boldsymbol{\theta}_{\mathcal{N}_2}))}, \cdots, e^{j\angle(\boldsymbol{a}_{N,T}^{\mathrm{H}}(\boldsymbol{p},f_s)\,\boldsymbol{w}^{\mathrm{ps}}(\boldsymbol{\theta}_{\mathcal{N}_T}))}\big)\,. \tag{27}$$

We provide a brief overview of fundamental concepts from differential geometry. A Riemannian manifold $(\mathcal{M}, g)$ is a smooth manifold $\mathcal{M}$ equipped with a smoothly-varying family g of positive-definite inner products (i.e., Riemannian metric) on the tangent space $\mathcal{T}_{\boldsymbol{p}}\mathcal{M}$ at each point $\boldsymbol{p} \in \mathcal{M}$. A smooth manifold $\mathcal{M}$ is a topological space that locally behaves like Euclidean space and possesses a smooth structure. The tangent space $\mathcal{T}_{\boldsymbol{p}}\mathcal{M} \triangleq \{\gamma'(\boldsymbol{0}) \mid \gamma : \mathcal{I}(\subseteq \mathbb{R}) \to \mathcal{M}\gamma(\boldsymbol{0}) = \boldsymbol{p}\}$ is a vector space containing tangent vectors at $\boldsymbol{p}$. It has been shown that the tangent space of $\mathcal{C}^T$ is given by

$$\mathcal{T}_{\tilde{\boldsymbol{\tau}}}\,\mathcal{C}^T = \big\{\boldsymbol{p} \in \mathbb{C}^T \mid \Re\big\{[\boldsymbol{p}]_i^* [\tilde{\boldsymbol{\tau}}]_t\big\} = 0,\ \forall t\big\}\,. \tag{28}$$

We now describe the Riemannian conjugate gradient (RCG) method for solving $\mathscr{P}_{2,\mathrm{b}}$. Unlike the traditional conjugate gradient method, it involves two additional steps to find the optimal solution on the manifold: 1) *projection* which projects the search direction onto the tangent space, and 2) *retraction* which maps the updated point back onto the manifold.

Lemma 1. *The orthogonal projection* $\mathrm{proj}_{\mathcal{T}_{\tilde{\boldsymbol{\tau}}}\mathcal{C}^T} : \mathbb{C}^T \to \mathcal{T}_{\tilde{\boldsymbol{\tau}}}\mathcal{C}^T$ *onto the tangent space* $\mathcal{T}_{\tilde{\boldsymbol{\tau}}}\mathcal{C}^T$ *at* $\tilde{\boldsymbol{\tau}} \in \mathcal{C}^T$ *is defined as follows [16]:*

$$\mathrm{proj}_{\mathcal{T}_{\tilde{\boldsymbol{\tau}}}\mathcal{C}^T}(\boldsymbol{p}) = \boldsymbol{p} - \Re\big\{\boldsymbol{p}^* \odot \tilde{\boldsymbol{\tau}}\big\} \odot \tilde{\boldsymbol{\tau}} \quad \forall \boldsymbol{p} \in \mathbb{C}^T\,. \tag{29}$$

By applying the projection operator, we can determine the Riemannian gradient, which represents the direction of steepest descent for f_{b} within the tangent space. Since $\mathcal{C}^T$ is embedded in $\mathbb{C}^T$, the Riemannian gradient is computed by projecting the Euclidean gradient onto the tangent space.

Lemma 2. *Let* f_{b} *be the objective function of* $\mathscr{P}_{2,\mathrm{b}}$. *Then the Riemannian gradient* $\mathrm{grad}\, f_{\mathrm{b}}(\tilde{\boldsymbol{\tau}})$ *of* f_{b} *at* $\tilde{\boldsymbol{\tau}} \in \mathcal{C}$ *can be obtained by projecting the complex Euclidean gradient* $\nabla_{\tilde{\boldsymbol{\tau}}} f_{\mathrm{b}}(\tilde{\boldsymbol{\tau}})$ *onto the tangent space* $\mathcal{T}_{\tilde{\boldsymbol{\tau}}}\mathcal{C}$ *as [16]*

$$\mathrm{grad}\, f_{\mathrm{b}}(\tilde{\boldsymbol{\tau}}) = \nabla_{\tilde{\boldsymbol{\tau}}} f_{\mathrm{b}}(\tilde{\boldsymbol{\tau}}) - \Re\big\{\nabla_{\tilde{\boldsymbol{\tau}}} f_{\mathrm{b}}^*(\tilde{\boldsymbol{\tau}}) \odot \tilde{\boldsymbol{\tau}}\big\} \odot \tilde{\boldsymbol{\tau}}\,. \tag{30}$$

Lemma 3. *The retraction* $\mathrm{retr}_{\tilde{\boldsymbol{\tau}}} : \mathcal{T}_{\tilde{\boldsymbol{\tau}}}\mathcal{C}^T \to \mathcal{C}^T$ *onto* $\mathcal{C}^T$ *at* $\tilde{\boldsymbol{\tau}} \in \mathcal{C}^T$ *is defined as follows for all* $\boldsymbol{v} \in \mathcal{T}_{\tilde{\boldsymbol{\tau}}}\mathcal{C}$ *[16]:*

$$\mathrm{retr}_{\tilde{\boldsymbol{\tau}}}(\boldsymbol{v}) = \left[\frac{[\tilde{\boldsymbol{\tau}}+\boldsymbol{v}]_1}{|[\tilde{\boldsymbol{\tau}}+\boldsymbol{v}]_1|}\ \frac{[\tilde{\boldsymbol{\tau}}+\boldsymbol{v}]_2}{|[\tilde{\boldsymbol{\tau}}+\boldsymbol{v}]_2|}\ \cdots\ \frac{[\tilde{\boldsymbol{\tau}}+\boldsymbol{v}]_T}{|[\tilde{\boldsymbol{\tau}}+\boldsymbol{v}]_T|}\right]^{\mathrm{T}}. \tag{31}$$

The update equations for the conjugate direction $\boldsymbol{d}_i \in \mathcal{C}^T$ and $\tilde{\boldsymbol{\tau}}_i$ at the ith iteration are given by

$$\boldsymbol{d}_i = \mathrm{grad}\, f_{\mathrm{b}}(\tilde{\boldsymbol{\tau}}_i) + \beta_i \mathrm{proj}_{\mathcal{T}_{\tilde{\boldsymbol{\tau}}_i}\mathcal{C}^T}(\boldsymbol{d}_{i-1}) \tag{32}$$
$$\tilde{\boldsymbol{\tau}}_{i+1} = \mathrm{retr}_{\tilde{\boldsymbol{\tau}}_i}(\alpha_i \boldsymbol{d}_i)\,. \tag{33}$$

Here, α_i is the step size determined by the line search method, and $\beta_i = \frac{\|\mathrm{grad}\, f_{\mathrm{b}}(\tilde{\boldsymbol{\tau}}_i)\|_2^2}{\|\mathrm{grad}\, f_{\mathrm{b}}(\tilde{\boldsymbol{\tau}}_{i-1})\|_2^2}$ is the Fletcher-Reeves conjugate gradient parameter. In (32), the projection operator is applied because $\boldsymbol{d}_{i-1}$ lies in the tangent space $\mathcal{T}_{\tilde{\boldsymbol{\tau}}_{i-1}}\mathcal{C}^T$ of $\tilde{\boldsymbol{\tau}}_{i-1}$. Also,

in (33), the retraction operator ensures that $\tilde{\boldsymbol{\tau}}_i$ remains within $\mathcal{C}^T$. The update steps in (32) and (33) are repeated until $\tilde{\boldsymbol{\tau}}_i$ converges. Once the optimal solution $\tilde{\boldsymbol{\tau}}^{\mathrm{opt}}$ is found, we obtain the TTD time delay as $\tau_t^{\mathrm{opt}} = -\frac{1}{f_c}\angle\tilde{\tau}_t^{\mathrm{opt}}$.

D. PS Phase Shift Optimization

For a given $(\boldsymbol{\pi}, \boldsymbol{\tau}) = (\boldsymbol{\pi}^{\mathrm{opt}}, \boldsymbol{\tau}^{\mathrm{opt}})$, $\mathscr{P}_0$ is reduced to the phase shift control problem $\mathscr{P}_{0,\mathrm{c}}$ as

$$\mathscr{P}_{0,\mathrm{c}}: \underset{\{\boldsymbol{\theta}_{\mathcal{N}_t}\}_{t=1}^T}{\text{maximize}} \sum_{s=1}^{S}\left|\sum_{t=1}^{T} m_{s,t}e^{jv_{s,t}}\right|^2 \tag{34a}$$

$$\text{subject to } m_{s,t} = \left|\boldsymbol{a}_{N,t}^{\mathrm{H}}(\boldsymbol{p}, f_s)\,\boldsymbol{w}^{\mathrm{ps}}(\boldsymbol{\theta}_{\mathcal{N}_t})\right| \quad \forall s \in \mathcal{S}, \forall t \in \mathcal{T} \tag{34b}$$

$$v_{s,t} = -2\pi f_s \tau_t^{\mathrm{opt}} + \angle(\boldsymbol{a}_{N,t}^{\mathrm{H}}(\boldsymbol{p}, f_s)\,\boldsymbol{w}^{\mathrm{ps}}(\boldsymbol{\theta}_{\mathcal{N}_t})) \quad \forall s \in \mathcal{S}, \forall t \in \mathcal{T}\,. \tag{34c}$$

Unfortunately, it is not possible to directly decompose $\mathscr{P}_{0,\mathrm{c}}$ into subproblems for each $\boldsymbol{\theta}_{\mathcal{N}_t}$ because (34a) is a joint function of $\{\boldsymbol{\theta}_{\mathcal{N}_t}\}_{t=1}^T$. To resolve this, we adopt a two-stage approach: 1) determine $\{m_{s,t}, v_{s,t}\}$ that maximizes (34a), and 2) individually solve for each $\boldsymbol{\theta}_{\mathcal{N}_t}$ that satisfies (34b) and (34c). First, by relaxing (34b) and (34c), the optimization problem for $\{m_{s,t}, v_{s,t}\}$ is formulated as follows:

$$\mathscr{P}_{1,\mathrm{c}}: \quad \underset{\{m_{s,t}, v_{s,t}\}_{s,t}}{\text{maximize}} \quad \sum_{s=1}^{S}\left|\sum_{t=1}^{T} m_{s,t}e^{jv_{s,t}}\right|^2 \tag{35a}$$

$$\text{subject to} \quad 0 \leqslant m_{s,t} \leqslant |\mathcal{N}_t| \qquad \forall t \in \mathcal{T}\,. \tag{35b}$$

One can easily see the optimal solution for $\mathscr{P}_{1,\mathrm{c}}$ is given by $m_{s,t}^{\mathrm{opt}} = |\mathcal{N}_t|$ and $v_{s,t}^{\mathrm{opt}} = 0$. Using these, we determine $\{\boldsymbol{\theta}_{\mathcal{N}_t}\}_{t=1}^T$ that satisfy (34b) and (34c). Since (34b) and (34c) are functions only of $\boldsymbol{\theta}_{\mathcal{N}_t}$, the phase shift control problem can be decoupled into subproblems for each $\boldsymbol{\theta}_{\mathcal{N}_t}$ as

$$\mathscr{P}_{2,\mathrm{c},t}: \underset{\boldsymbol{\theta}_{\mathcal{N}_t}}{\text{minimize}} \sum_{s=1}^{S}\left|\boldsymbol{a}_{N,t}^{\mathrm{H}}(\boldsymbol{p}, f_s)\,\boldsymbol{w}^{\mathrm{ps}}(\boldsymbol{\theta}_{\mathcal{N}_t}) - |\mathcal{N}_t| e^{j2\pi f_s \tau_t^{\mathrm{opt}}}\right|^2 \tag{36}$$

Similar to the time delay optimization, we redefine the optimization variable as $\tilde{\boldsymbol{\theta}}_{\mathcal{N}_t} = [e^{-j\theta_n} \mid n \in \mathcal{N}_t]^{\mathrm{T}} \in \mathbb{C}^{|\mathcal{N}_t|}$ and reformulate $\mathscr{P}_{2,\mathrm{c},t}$ as

$$\mathscr{P}_{3,\mathrm{c},t}: \underset{\tilde{\boldsymbol{\theta}}_{\mathcal{N}_t} \in \mathcal{C}^{|\mathcal{N}_t|}}{\text{minimize}} \sum_{s=1}^{S}\left|\boldsymbol{a}_{N,t}^{\mathrm{H}}(\boldsymbol{p}, f_s)\,\tilde{\boldsymbol{\theta}}_{\mathcal{N}_t} - |\mathcal{N}_t| e^{j2\pi f_s \tau_t^{\mathrm{opt}}}\right|^2. \tag{37}$$

The optimal solution of $\mathscr{P}_{3,\mathrm{c},t}$ can be obtained via the RCG method. Then we get the PS phase shift as $\theta_n^{\mathrm{opt}} = -\angle\tilde{\theta}_n^{\mathrm{opt}}$. The subarray connection, and time delay and phase shift optimizations are repeated until $(\boldsymbol{\pi}, \boldsymbol{\tau}, \{\boldsymbol{\theta}_{\mathcal{N}_t}\}_{t=1}^T)$ converges.

IV. Numerical Results

A. Simulation Setup

In our simulations, we consider a wideband THz ELAA system where a BS with $N = 256$ antennas serves a single-antenna UE by generating frequency-dependent beams $\{\boldsymbol{w}_s\}_{s=1}^S$ directed towards the UE. The UE is randomly placed around the BS within a cell radius of $R = 100\,\mathrm{m}$. The number of TTDs and PS subarrays are set to $T = 4$ and $L = 64$, respectively. Note that the number of PSs matches the number of antennas N, meaning each PS subarray contains $K = \frac{N}{L} = 4$ PSs. We use a frequency-selective geometric THz channel model with a carrier frequency of $f_c = 100\,\mathrm{GHz}$, a bandwidth of $B = 20\,\mathrm{GHz}$, and $S = 128$ subcarriers. The number of propagation paths is $N_{\mathrm{p}} = 4$. As performance metrics, we use the sum of squares of array gains $G_{\mathrm{sum}} = \frac{1}{N^2}\sum_{s=1}^{S}|\boldsymbol{a}_N^{\mathrm{H}}(\boldsymbol{p}, f_s)\,\boldsymbol{w}_s|^2$ and the data rate $\mathsf{R} = \frac{1}{S}\sum_{s=1}^{S}\log_2\left(1 + \frac{P_{\mathrm{tx}}}{\sigma^2}|\mathbf{h}_s^{\mathrm{H}}\boldsymbol{w}_s|^2\right)$.

For comparison, we use four benchmark schemes: 1) the fully-digital approximation (FDA) scheme, which iteratively optimizes both $\boldsymbol{\tau}$ and $\boldsymbol{\theta}$ [11]; 2) the dynamic-subarray with fixed TTD (DS-FTTD) scheme, which utilizes a dynamic subarray architecture between TTDs and PSs with fixed TTD time delays [12]; 3) the phase-delay focusing (PDF) scheme, which controls the TTD time delays and PS phase shifts according to (7) [10]; and 4) the PS-based beamforming scheme, which generates a frequency-invariant beamforming vector that is the same for all subcarriers.

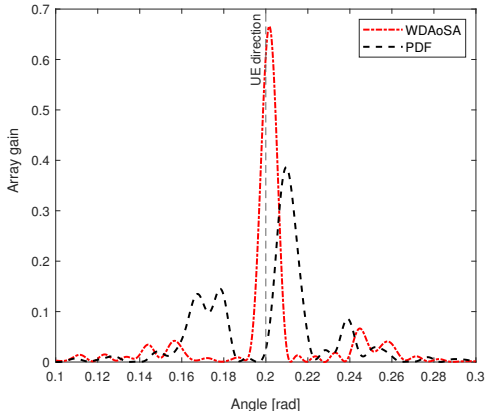

Fig. 2: Array gain as a function of the angle.

B. Simulation Results

In Fig. 2, the UE is positioned at $(r^{\mathrm{ue}}, \phi^{\mathrm{ue}}) = (10\,\mathrm{m}, 0.2\,\mathrm{rad})$, and we plot the power of the array gain $|G(\boldsymbol{w}_1, \boldsymbol{p})|^2 = \frac{1}{N^2}|\boldsymbol{a}_N^{\mathrm{H}}(\boldsymbol{p}, f_1)\,\boldsymbol{w}_1|^2$ for the 1st subcarrier as a function of the angle ϕ of $\boldsymbol{p} = [\,r\cos\phi\; r\sin\phi\,]^{\mathrm{T}}$, with r fixed at $r = r^{\mathrm{ue}}$. We observe that the proposed WDAoSA scheme achieves an array gain of 0.7 near the UE direction (i.e., $\phi^{\mathrm{ue}} = 0.2\,\mathrm{rad}$). Given that the frequency difference between f_1 and f_c is nearly 10 GHz, the substantial array gain improvement achieved by WDAoSA is rather unexpected. In contrast, the conventional PDF scheme exhibits a significantly lower array gain compared to WDAoSA. Moreover, the direction at which PDF achieves its maximum array gain is notably misaligned with the UE direction, indicating that the PDF beam is not properly directed toward the UE.

In Fig. 3, we plot the sum of squares of array gains G_{sum} as a function of system bandwidth B. The proposed WDAoSA scheme shows a significant improvement in array gain com-

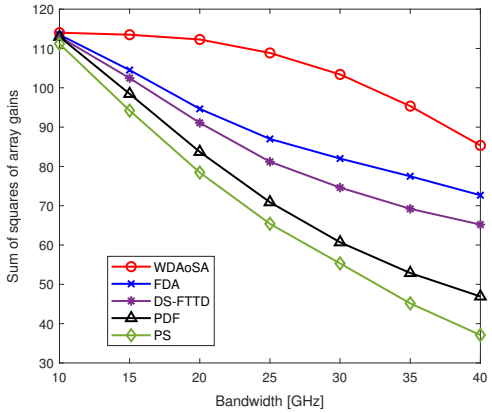

Fig. 3: Sum of squares of array gains as a function of the system bandwidth.

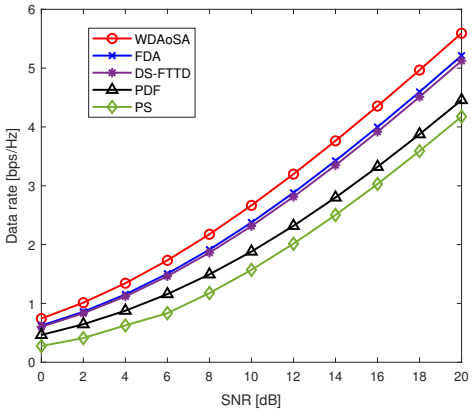

Fig. 4: Data rate as a function of SNR.

pared to conventional TTD-based beamforming schemes. Furthermore, the array gain enhancement of WDAoSA increases with larger system bandwidths. For example, when $B = 15\,\text{GHz}$, WDAoSA achieves an array gain improvement of about 8.5% over the FDA scheme, which increases to 27.6% when $B = 40\,\text{GHz}$. As bandwidth increases, the gap between carrier and subcarrier frequencies widens, leading to a larger mismatch between the optimal and generated beams. While WDAoSA dynamically adjusts the connections between TTDs and PSs subarrays to mitigate this mismatch, the FDA scheme lacks such a mechanism, resulting in array gain degradation.

In Fig. 4, we show the data rate as a function of signal-to-noise ratio (SNR). The proposed WDAoSA scheme consistently outperforms conventional TTD-based beamforming approaches. For instance, at SNR $= 20\,\text{dB}$, WDAoSA achieves data rate gains of approximately 11%, 31%, and 39% over the DS-FTTD, PDF, and PS-based beamforming schemes, respectively. Even compared to the FDA scheme, WDAoSA provides a data rate gain of about 10%. This strong data rate performance of WDAoSA can be attributed to two main factors: 1) the signal power in mmWave and THz bands is primarily concentrated along the line-of-sight (LoS) path, and 2) WDAoSA generates highly focused beams precisely directed toward the UE.

V. Conclusion

In this paper, we introduced a TTD-based wideband beamforming scheme called WDAoSA, which dynamically reconfigures the connections between TTDs and PS subarrays through a switch network. Unlike conventional TTD-based beamforming schemes, where fixed subarray connections result in unavoidable sidelobe leakage and array gain degradation in subcarrier beams, WDAoSA optimizes the subarray connections, TTD time delays, and PS phase shifts to maximize array gain. To achieve this, we developed both centralized and distributed beamforming optimization techniques that jointly adjust the subarray connections, TTD time delays, and PS phase shifts. Numerical results show that WDAoSA provides over 40% improvement in array gain compared to conventional TTD-based beamforming schemes.

References

[1] E. G. Larsson, O. Edfors, F. Tufvesson, and T. L. Marzetta, "Massive MIMO for next generation wireless systems," *IEEE Commun. Mag.*, vol. 52, no. 2, pp. 186–195, Feb. 2014.

[2] M. Chiani, M. Z. Win, and H. Shin, "MIMO networks: The effects of interference," *IEEE Trans. Inf. Theory*, vol. 56, no. 1, pp. 336–349, Jan. 2010.

[3] J. H. Winters, "Optimum combining in digital mobile radio with cochannel interference," *IEEE J. Sel. Areas Commun.*, vol. SAC-2, no. 4, pp. 528–539, Jul. 1984.

[4] A. Conti, W. M. Gifford, M. Z. Win, and M. Chiani, "Optimized simple bounds for diversity systems," *IEEE Trans. Commun.*, vol. 57, no. 9, pp. 2674–2685, Sep. 2009.

[5] J. H. Winters, "Optimum combining for indoor radio systems with multiple users," *IEEE Trans. Commun.*, vol. COM-35, no. 11, pp. 1222–1230, Nov. 1987.

[6] B. Wang, M. Jian, F. Gao, G. Y. Li, and H. Lin, "Beam squint and channel estimation for wideband mmWave massive MIMO-OFDM systems," *IEEE Trans. Sig. Process.*, vol. 67, no. 23, pp. 5893–5908, Dec. 2019.

[7] L. Dai, J. Tan, Z. Chen, and H. V. Poor, "Delay-phase precoding for wideband THz massive MIMO," *IEEE Trans. Wireless Commun.*, vol. 21, no. 9, pp. 7271–7286, Sep. 2022.

[8] S. Kim, J. Park, J. Moon, and B. Shim, "Fast and accurate terahertz beam management via frequency-dependent beamforming," *IEEE Trans. Wireless Commun.*, vol. 23, no. 3, pp. 4457–4469, Mar. 2024.

[9] F. Gao, B. Wang, C. Xing, J. An, and G. Y. Li, "Wideband beamforming for hybrid massive MIMO terahertz communications," *IEEE J. Sel. Areas Commun.*, vol. 39, no. 6, pp. 1725–1740, Jun. 2021.

[10] M. Cui and L. Dai, "Near-field wideband beamforming for extremely large antenna arrays," *IEEE Trans. Wireless Commun.*, vol. 23, no. 10, pp. 13 110–13 124, Oct. 2024.

[11] Z. Wang, X. Mu, and Y. Liu, "Beamfocusing optimization for near-field wideband multi-user communications," *IEEE Trans. Commun.*, vol. 73, no. 1, pp. 555–572, Jan. 2025.

[12] L. Yan, C. Han, and J. Yuan, "Energy-efficient dynamic-subarray with fixed true-time-delay design for terahertz wideband hybrid beamforming," *IEEE J. Sel. Areas Commun.*, vol. 40, no. 10, pp. 2840–2854, Oct. 2022.

[13] S. Kim, J. Moon, J. Wu, B. Shim, and M. Z. Win, "Vision-aided positioning and beam focusing for 6G terahertz communications," *IEEE J. Sel. Areas Commun.*, vol. 42, no. 9, pp. 2503–2519, Sep. 2024, special issue on *Positioning and Sensing Over Wireless Networks*.

[14] E. J. Candes, M. B. Wakin, and S. P. Boyd, "Enhancing sparsity by reweighted l_1 minimization," *J. Fourier Anal. Appli.*, vol. 14, no. 5-6, pp. 877–905, Oct. 2008.

[15] S. Kim, J. Wu, B. Shim, and M. Z. Win, "Cell-free massive non-terrestrial networks," *IEEE J. Sel. Areas Commun.*, vol. 43, no. 1, pp. 201–217, Jan. 2025, special issue on *Integrated Ground-Air-Space Wireless Networks for 6G Mobile*.

[16] P.-A. Absil, R. Mahony, and R. Sepulchre, *Optimization algorithms on matrix manifolds*. Princeton, NJ, USA: Princeton Univ. Press, 2009.